Int. J. Electrochem. Sci., 17 **(2022)** Article Number: 22027, doi: 10.20964/2022.02.35

International Journal of
ELECTROCHEMICAL
SCIENCE
www.electrochemsci.org

Influence of Calcium Nitrite on Electrochemical Corrosion Behavior of API X120 Carbon Steel and 316LN Stainless Steel Reinforced Concrete in Marine Environment

Liao Jinsong, Gao Qian[*]*, Li Jing, Fan Lin*

Department of Construction Management and Real Estate, Chongqing Jianzhu College, Chongqing, 400072, China
[*]E-mail: gao.qian21@protonmail.com; li89561zhang58@163.com

Received: 20 October 2021 / *Accepted:* 30 November 2021 / *Published:* 5 January 2022

This study was carried out to evaluate the corrosion behavior of API X120 carbon steel and 316LN stainless steel reinforced concrete in marine environments with calcium nitrite as an inhibitor. The electrochemical impedance spectroscopy (EIS) technique and SEM were applied to study the concentration effect of calcium nitrite on the corrosion behavior of API X120 carbon steel and 316LN stainless steel reinforced concrete in a 3.5%wt NaCl solution containing calcium nitrite at pH values of 8, 10 and 12. Results showed that double-layer capacitance decreases and charge-transfer resistance increases by increasing the inhibitor concentration which is associated with improvement of the 'blanketing' property of the film. The surface coverage and inhibition efficiency also increase with an increase in inhibitor concentration. A calcium nitrite concentration of 50 µM showed 87.7% and 93% inhibition efficiency at pH 12 at room temperature for API X120 carbon steel and 316LN stainless steel, respectively. A comparison between the electrochemical corrosion behavior of API X120 carbon steel and 316LN stainless steel reinforced concrete revealed a remarkable decrease in the lifetime of the structure and damage due to reinforcement corrosion of API X120 carbon steel, indicating an increase in the cost associated with monitoring and maintenance. Therefore, replacing the API X120 carbon steel reinforcement with 316LN stainless steel can decrease the corrosion rate and can also considerably decrease the costs related to expensive equipment for rehabilitation.

Keywords: API X120 carbon steel; 316LN stainless steel; Electrochemical impedance spectroscopy; Calcium nitrite; Inhibitor; Corrosion

1. INTRODUCTION

Today, concrete is an important modern construction material and is used in the construction of huge buildings, bridges, roads, sidewalks, flooring, etc. because of its strength, stability, inexpensive, flexibility, versatility and mouldability [1]. Concrete becomes the matrix while steel bars or wires

provide the reinforcement so that the reinforcing steel-rods, bars, or mesh can absorb the tensile, shear, and sometimes compressive stresses in a concrete structure [2, 3]. Reinforced concrete is used for construction on a large scale, such as bridges, dams, piers, dams, tall buildings and stadiums [4, 5]. Numerous reinforced concrete structures in a marine environment such as bridges, piers and offshore platforms, are exposed to aggressive chloride ions [6, 7]. This causes the corrosion after short service periods, as consequently the underwater concrete coated pipelines also suffer the same problem.

Hundreds of billions of pounds are spent each year on repairing and replacing concrete structures around the world. Bridges in marine environments suffer from severe corrosion, which is linked to the production of cracks, over the course of their service lives [8]. Temperature fluctuations, foundation collapse owing to soft clay brick decay, concrete erosion due to chemical pollutants, and ground movement due to clay shrinkage, landslip, vibration, subsidence, and sway are the most prevalent causes of cracking. Long-term, these cracks allow chloride and CO_2 to migrate into the concrete, resulting in aggressive chloride assault [9]. Furthermore, corrosion of the steel reinforcing bars might occur either to localized failure of the passive coating on the steel due to chloride ions or a widespread failure of the passivity due to concrete neutralization due to reactivity with carbon dioxide from the atmosphere [10]. As a result, the steel's passive layer is broken, resulting in corrosion and cavities on the surface [11]. Because rust takes up more space than steel, it exerts internal pressure on the surrounding concrete, causing it to crack and deteriorate. Steel corrosion affects the effective cross section of structural components, causing the structures' seismic capacity to deteriorate with time [12].

Accordingly, the cost of repairing and replacing deteriorated structures has become a big problem [13, 14]. Chlorides lead to corrosion of steel inside concrete, cracking, delamination and spalling [15, 16]. pH value, moisture, oxygen, carbonation, ambient temperature and relative humidity are the environmental factors which generally influence corrosion of reinforcement [17-19]. Therefore, many studies were conducted to investigate the effect of environmental conditions on the corrosion rate of different reinforcing steels, identify the corrosion threats, and determine the suitable inhibitors [20-22]. Inhibitors are chemical compositions of organic-inorganic materials that are absorbed by the metal surface and form a protective oxide film on the surface of the metal causing the shift forces the metallic surface into the passivation region and decrease the corrosion rate [23, 24]. Among the inhibiters, nitrite as an anodic inhibitor can increase anodic polarization, and adsorb on the surface to form an inhibitive film as a barrier between electrolytic solution and metal to stop the corrosion reaction [25, 26].

Calcium nitrite, one of the various nitrite inhibitors, can be a cost-effective, straightforward, and appealing way to stop or reduce chloride-induced corrosion in reinforced concrete [27, 28]. They compete with chloride ions in the reaction with ferrous ions released from steel, promoting the creation of ferric oxide (Fe_2O_3), which is then transformed to more stable ferric oxide (FeOOH) in the passive layer as a result of the processes that follow [26].

$$2Fe^{2+} + 2OH^- + 2NO_2^- \rightarrow 2NO + Fe_2O_3 + H_2O \quad (1)$$

$$Fe^{2+} + 2OH^- + 2NO_2^- \rightarrow NO + \gamma\text{-FeOOH} \quad (2)$$

Furthermore, the concrete's strong alkaline conditions, with pH values ranging from 12 to 14, allow for the production of a passive layer that functions as a protective coat and prevents the steel reinforcement from corroding [29]. The interaction of the breakdown and hydrolysis products of the

bicarbonate ion of sea water with calcium ions to form $CaCO_3$ is said to cause the alkalinity of concrete in the marine environment. This salt builds up and blocks the pores, preventing the harsh environment from penetrating further into the concrete [30, 31]. Furthermore, Ca^{2+} ions can migrate to the metal surface's cathodic area and create $Ca(OH)_2$ through an interaction with hydroxyl ions (OH-) [32]. Moreover, it is suggested that Ca(OH)2 inhibition is dependent on increasing pH (12), which leads to the formation of a barrier layer of calcium ions in the water as carbonate and/or sulfate on the surface, which can provide excellent corrosion protection in marine environments and saline solutions [33].

Few research on long-term corrosion of reinforced concrete in marine environments have been conducted [34-37], particularly on the effect of calcium nitrite as an inhibitor and the comparison of API X120 carbon steel and 316LN stainless steel. Therefore, this study was carried out to evaluate the corrosion behavior of API X120 carbon steel and 316LN stainless steel reinforced concrete in marine environment with calcium nitrite as an inhibitor.

2. MATERIALS AND METHOD

The reinforced concrete was prepared from a mixture of ordinary portland cement type I (OPC-I, Vietnam Trading Investment and Import Export Jsc., Vietnam), distilled water, sand (EN 196-1 standard sand, Hangzhou Civit Instrument Equipment Co., Ltd., China), and 50 mm maximum size river coarse aggregates. Table 1 presents the mix proportion of concrete material and the resultant compressive strength, which were used for the preparation of a set of 15 cm concrete cube samples. The test specimens with 1.2 cm diameter steel bars were embedded in the center of the prepared concrete cube molds to produce working electrodes. A schematic diagram of the cells configured for the EIS experiment is shown in Figure 1.

The chemical composition of steel bars was summarized in the Table 2. Only a half of the length of steel bars were embedded in concrete to make sure the bond slip failure dominated over other types of failure.

Electrochemical studies were conducted in 3.5% wt NaCl (≥99.0%, Sigma-Aldrich) solution with pH 12. The calcium nitrite (≥99.0%, Sigma-Aldrich) as an inhibitor was added to the 3.5%wt NaCl solution (5, 15, 25 and 50 μM). The pH of electrochemical solution was adjusted at ranges from 8 to 12 using a Horiba pH meter (Laqua, 9618S-10D, Horiba, Japan) by adding 0.01 M NaOH (99.0%, Sigma-Aldrich) and 0.01 M HCl (99.0%, Sigma-Aldrich). Furthermore, the reinforced concrete samples were immersed in a marine environment for up to four months to determine the scheme of embedded steel in the concrete and the formation of cracks over time due to chemical contaminants, temperature, carbon dioxide from the atmosphere, and chloride ion diffusion in reinforced concrete.

Table 1. The mix proportion of concrete material and resulted compressive strength.

Cement (kg/m^3)	**water (kg/m^3)**	**Sand (kg/m^3)**	**coarse aggregates (kg/m^3)**	**Compressive strength (MPa)**
451.5	203.8	811.9	987.5	46

Table 2. API X120 carbon steel and 316LN stainless steel chemical composition.

Element (wt %)	C	Mo	Ni	Mn	P	Si	Cr	S	others	Fe
API X120	0.129	0.0013	0.017	0.541	0.010	0.101	0.039	0.001	0.1	Balance
316LN	0.03	2	10	2.00	0.045	1.00	18	0.03	0.3	Balance

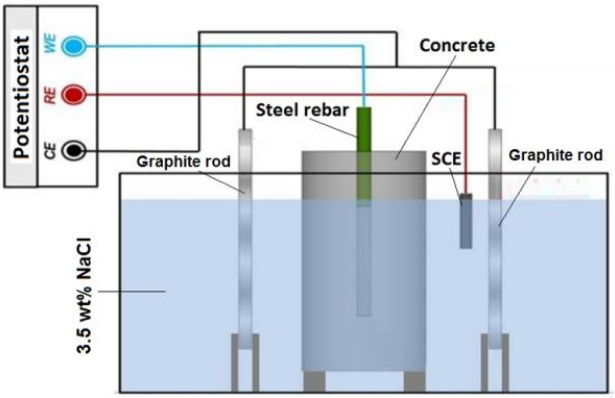

Figure 1. Schematic diagram of EIS experiment

Electrochemical analyses were conducted on potentiostat/galvanostat (CS1006, Zhengzhou CY Scientific Instrument Co., Ltd., China) using a three-electrode system which contained steel reinforced concrete as the working electrode, the saturated calomel electrode (SCE) as the reference electrode and a graphite rod as the auxiliary electrode. Electrochemical impedance spectroscopy (EIS) measurements were carried out in a potentiostat/galvanostat using AC signals with an amplitude of 10mV at open circuit potential and frequencies ranging from 10mHz to 100KHz. Analysis of the data was done using Zsim software and the equivalent circuit fitted to the EIS experimental data.

The scanning electron microscope (SEM; JXA-8100, JEOL Co. Ltd., Japan) was used for the surface morphological analysis of steel samples.

3. RESULTS AND DISCUSSION

EIS studies have been used to quantitatively analyze the electrode/electrolyte interfaces and describe the corrosion behavior [38]. The obtained Nyquist and Bode plots are depicted in Figures 2 and 3, respectively which related to API X120 carbon steel and 316LN stainless steel reinforced concrete in the presence of 5, 15, 25 and 50 μM of the calcium nitrite as corrosion inhibitor at room temperature in pH 8, 10 and 12. As observed from the Nyquist plots in Figure 2, the diameter of the semicircle increased with increasing pH of solution, indicating the promotion of the passivity of reinforcing steel by the alkalinity of concrete [23]. In addition, the Nyquist plot in intermediate frequencies doesn't exhibit a perfect semicircle because of the frequency dispersion phenomena and the roughness and inhomogeneity of the electrode surface [39].

Moreover, it can be observed from the Nyquist plots in Figure 2 and the Bode plots in Figures 3 and 4 that the diameter of the semicircle and capacitive loop diameter increase with an increasing in the calcium nitrite concentration, implying a decrease in the corrosion rate due to an increase in the adsorption of the inhibitor [27, 40]. The corrosion mechanism of chloride ions in reinforced concrete occurs through the destruction of passivation film and the electrochemical reaction of corrosion [26]. When the concentration of Cl^- in concrete reaches a certain level, Cl^- attack can be a main reason for localized corrosion of reinforcing steel in concrete and destruction of passivation film on the surface by pitting corrosion [41, 42]. The mechanism of destruction of passivation film by the presence of Cl^- or a reduction in alkalinity of concrete caused by carbonation [43]. The electrochemical corrosion reaction between Cl^- and the exposed cationic Fe^{2+} in the steel matrix can occur as the following reactions when the passive layer is destroyed [26, 41]:

$$Fe^{2+} + Cl^- \rightarrow Fe(OH)_2 + 2HCl \quad (3)$$

Nitrite, as a strong oxidizing agent and an anodic inhibitor, can oxidize the Fe atoms on the surface of steel and form Fe_2O_3, and can form an insoluble passivity layer on the surface of steel bar that inhibits the anodic reaction of the steel bar surface [27, 28]. Nitrite interferes with the anodic process (metal dissolution), and reduces the corrosion rate by suppressing the anodic reaction and inhibiting the micro-corrosion points in the passivation film into stable pitting through the formation or maintenance of a passive film on the metal surface as electrochemical reactions (1) and (2) between nitrite and Fe^{2+} form Fe_2O_3 [26].

Therefore, the electrochemical reactions increase the surface γ-FeOOH content in the passivation film, which can inhibit steel from localized corrosion [44]. According to research, nitrite has the ability to increase anodic polarization and thus decrease corrosion current and increase corrosion potential in a noble direction by preventing electron loss after the iron atoms continue to dissolve [25, 45]. As seen, the corrosion rate is relatively high at low concentrations of nitrite because the concentration is insufficient to passivate the entire surface of the steel bar. For a high concentration of nitrite, the electrochemical reactions (3) and (1) provide sufficient inhibition protection for reinforcement steel.

Furthermore, Figure 5 shows the schematic representation of a proposed equivalent circuit that is used to analyze EIS spectra and fit the experimental data. As observed from Figure 5, there is the two-time constant equivalent circuit, which is associated with analyzing an electrode undergoing uniform corrosion at open circuit [46]. The values for the elements of the equivalent circuits are summarized in Table 1. It contains the electrolyte resistance (R_s) between the working electrode and the reference electrode, charge transfer resistance across the metal surface (R_{ct}), resistance of the pores in the protective coating to the passage of electrolyte (R_{po}), double-layer capacitance (Cdl) at the electrode-solution interface, constant phase element of pore capacitance (CPE_{po}), constant phase element associated with the double layer capacitance (CPE_{ct}) [40]. n_1 and n_2 are deviation parameters from the ideal behavior which are attributed to the constant phase element because, as an equivalent electrical circuit component, it models the behavior of a non-ideal double layer as an imperfect capacitor [47].

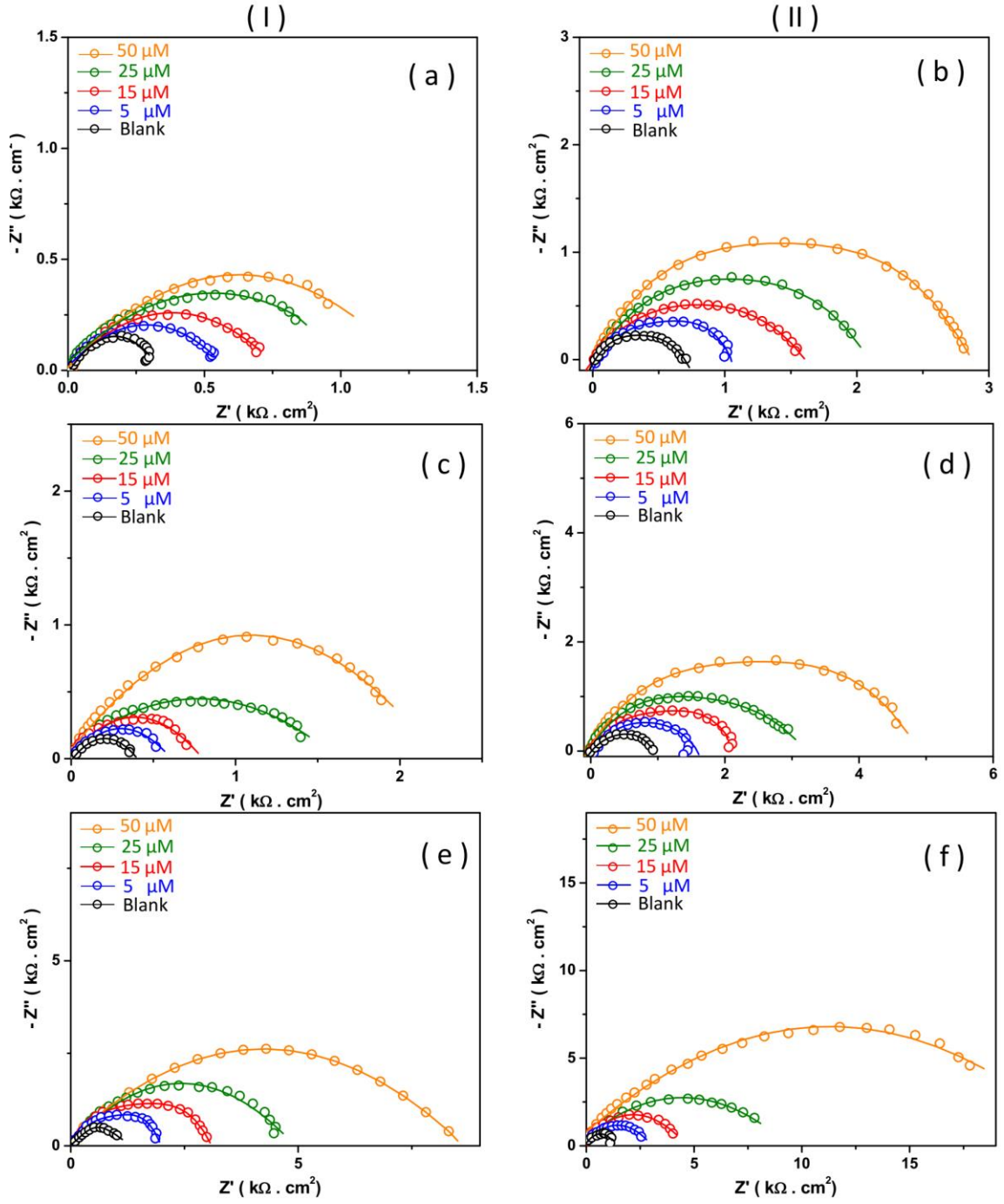

Figure 2. The obtained EIS Nyquist data (symbols) and fittings (solid lines) of API X120 carbon steel (column I) and 316LN stainless steel (column II) reinforced concrete in the presence of 5, 15, 25 and 50 µM of the calcium nitrite as corrosion inhibitor at room temperature (a and b) pH 8, (c and d) pH 10 and (e and f) pH 12.

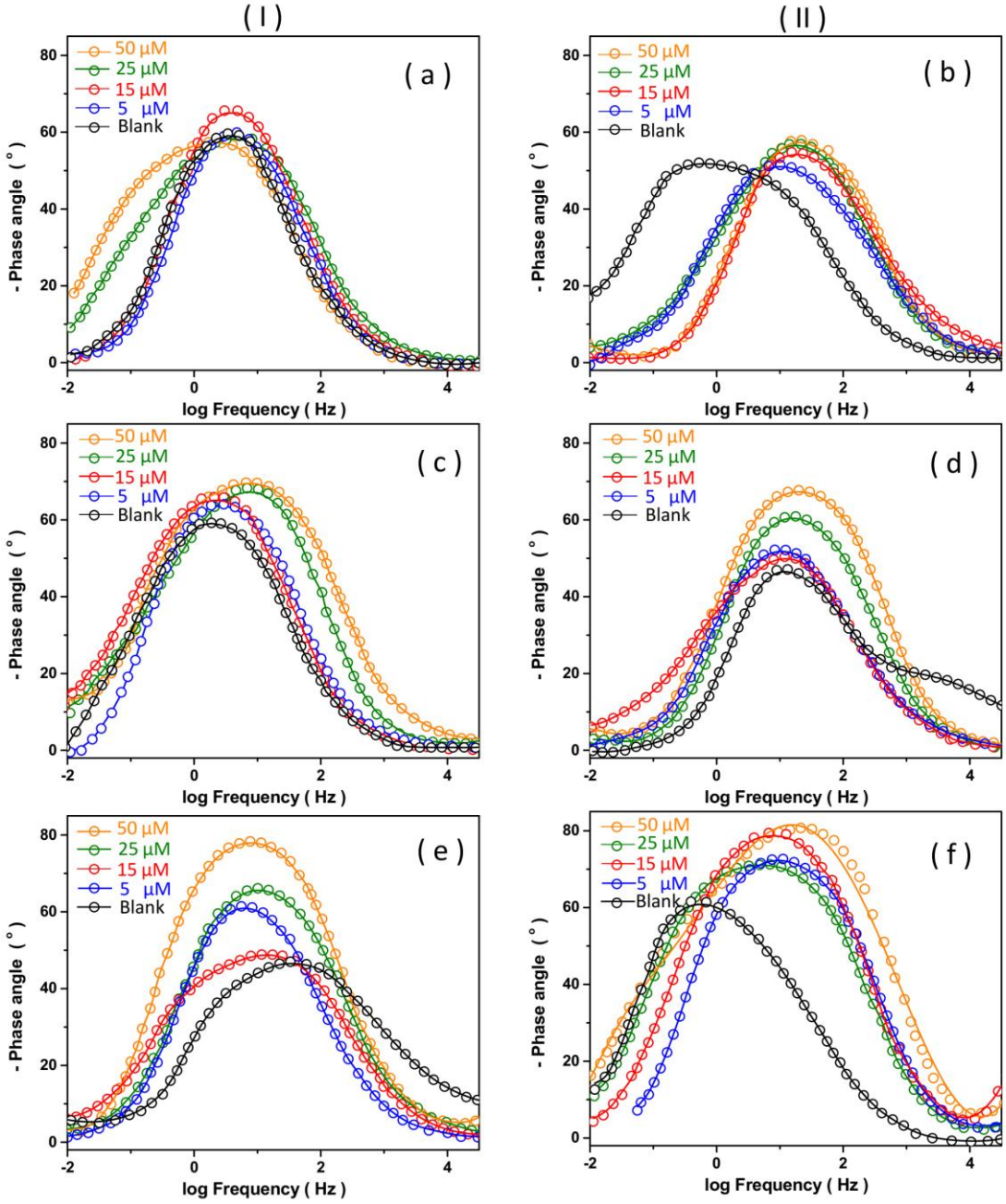

Figure 3. The obtained Bode plots of phase angle vs. log frequency data (symbols) and fittings (solid lines) of API X120 carbon steel (column I) and 316LN stainless steel (column II) reinforced concrete in the presence of 5, 15, 25 and 50 µM of the calcium nitrite as corrosion inhibitor at room temperature (a and b) pH 8, (c and d) pH 10 and (e and f) pH 12.

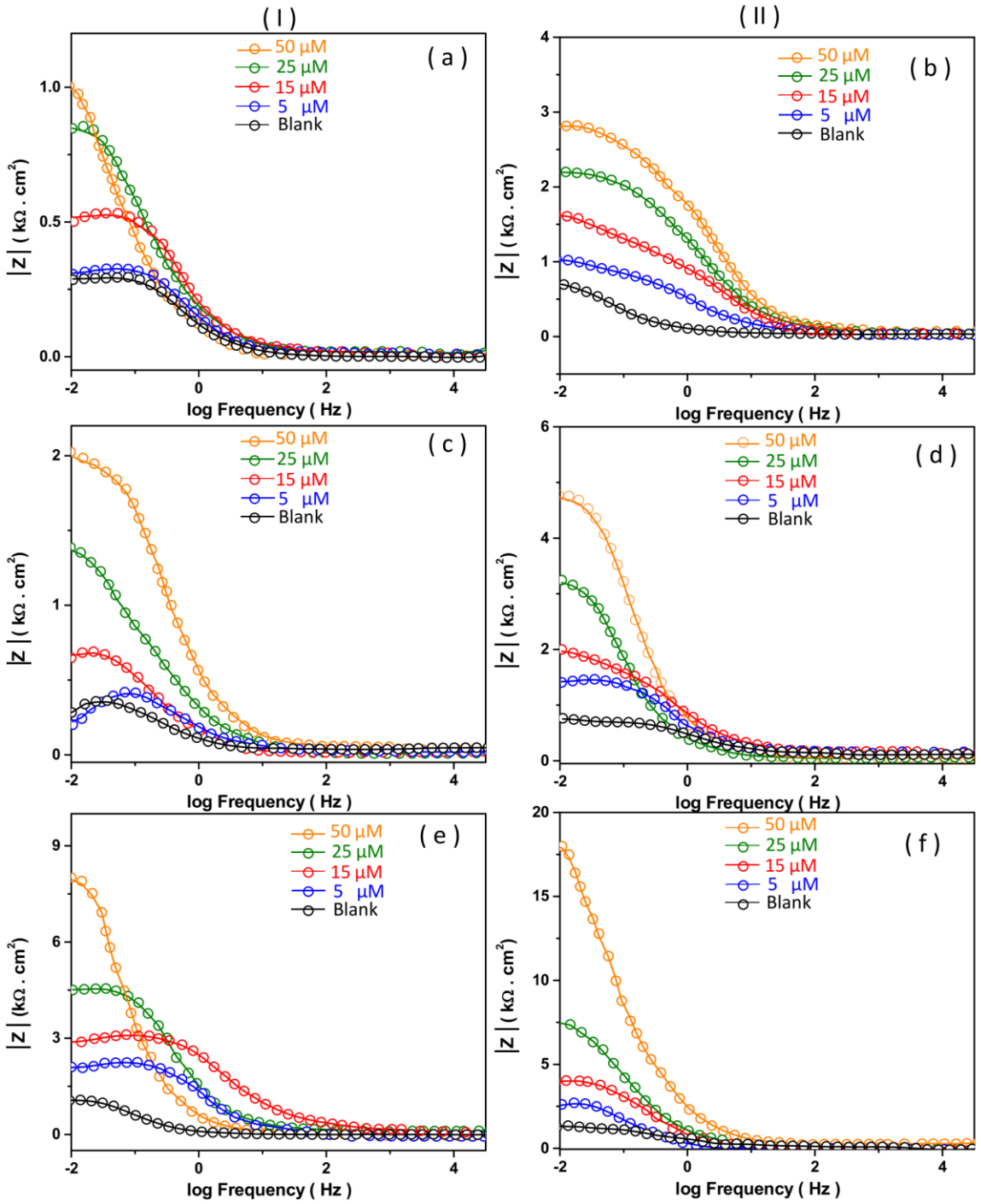

Figure 4. The obtained Bode plots of log |Z| *vs.* log frequency data (symbols) and fittings (solid lines) of API X120 carbon steel (column I) and 316LN stainless steel (column II) reinforced concrete in the presence of 5, 15, 25 and 50 µM of the calcium nitrite as corrosion inhibitor at room temperature (a and b) pH 8, (c and d) pH 10 and (e and f) pH 12.

The capacitance behavior is often related to the dielectric characteristics of the passive film of adsorbed inhibitor molecules or a surface corrosion product film [48, 49], and the imperfectness behavior is associated with surface roughness, non-uniform surface coverage, non-uniform thickness

of corrosion-inhibitor film, non-uniform current distribution or corrosion rate and porosity [50]. The impedance of CPE (Z_Q) can be determined by the following equation [51]:

$$Z_Q = \frac{1}{Q_0 (j\omega)^n} \quad (4)$$

Where Z_Q shows impedance of *CPE*(Ω cm^{-2}), Q_0 is the constant representative for CPE (Ω^{-1}cm^{-2}s^n), j represents imaginary number (j =$\sqrt{-1}$), $\omega = 2\pi f_{max}$ is the angular frequency (rad s^{-1}), f_{max} indicates the frequency at which the imaginary component reaches a maximum. The factor n, defined as a CPE power, is an adjustable parameter that mainly lies between 0 and 1. When n = 1, Q_0 has the constant representative of an ideal capacitor, and when n = 0, the CPE behaves as pure resistance [40, 51]. Tables 3 and 4 show the evaluated electrical parameters obtained by using EIS studies of API X120 carbon steel and 316LN stainless steel, respectively, where the surface coverage (θ) is the fraction of the total surface covered by inhibitor molecules [21], and inhibition efficiency (IE%) is expressed by equations (5) and (6), respectively [21, 51]:

$$\theta = \frac{R_{ct} - R_{ct}^o}{R_{ct}} \quad (5)$$

$$IE\ \% = \theta \times 100 \quad (6)$$

Where R_{ct} and R_{ct}^o are defined the charge-transfer resistance in presence and absence of calcium nitrite as corrosion inhibitor, respectively.

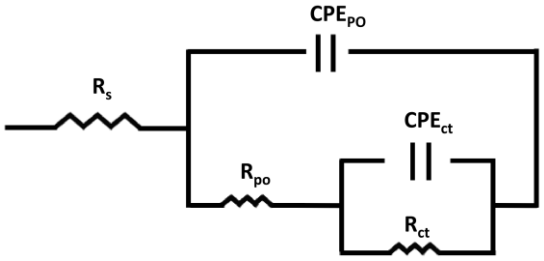

Figure 5. The schematic representation of a proposed equivalent circuit

Table 3. The evaluated electrical parameters obtained by using EIS studies of API X120 carbon steel.

pH	C_{inh}(µM)	Rs(Ω cm^{-2})	R_{po}(Ω cm^{-2})	*CPE*$_{po}$		R_{ct}(Ω cm^{-2})	*CPE*$_{ct}$		C_{dl}(µF cm^{-2})	θ	*IE*(%)
				$Q_{po} \times 10^{-6}$(s^n Ω^{-1} cm^{-2})	n_1		$Q_{ct} \times 10^{-6}$(s^n Ω^{-1} cm^{-2})	n_2			
8	Blank	7.33	–	–	–	289.11	821.33	0.588	309.93	–	–
	5	8.48	–	–	–	509.25	616.98	0.581	261.79	0.432	43.2
	15	8.98	–	–	–	708.52	412.30	0.680	230.24	0.591	59.1
	25	8.55	–	–	–	1038.25	229.25	0.849	180.41	0.721	72.1
	50	9.31	–	–	–	1207.22	124.02	0.848	90.10	0.760	76
10	Blank	8.37	22.89	819.42	0.817	338.11	451.33	0.796	279.85	-	-
	5	7.61	34.05	1330.15	0.760	648.21	360.25	0.765	230.51	0.478	47.8
	15	7.91	36.89	4155.60	0.979	901.24	279.11	0.801	200.12	0.624	62.4

pH	C_{inh}(μM)	Rs(Ω cm^{-2})	R_{po}(Ω cm^{-2})	CPE_{po}		R_{ct}(Ω cm^{-2})	CPE_{ct}		C_{dl}(μF cm^{-2})	θ	*IE*(%)
				$Q_{po} \times 10^{-6}$ (s^n Ω^{-1} cm^{-2})	n_1		$Q_{ct} \times 10^{-6}$ (s^n Ω^{-1} cm^{-2})	n_2			
	25	8.05	43.10	5002.31	0.528	1361.41	150.02	0.881	120.17	0.751	75.1
	50	8.62	52.11	5991.33	0.869	2158.31	100.14	0.651	42.98	0.843	84.3
12	Blank	6.81	52.71	1566.31	0.941	1002.32	179.50	0.798	120.12	-	-
	5	8.21	86.07	1187.25	0.650	1881.15	119.66	0.790	79.44	0.467	46.7
	15	6.57	216.78	809.11	0.881	2801.02	77.89	0.861	59.10	0.642	64.2
	25	4.51	372.89	571.32	0.590	4537.10	62.78	0.750	39.79	0.779	77.9
	50	6.07	624.98	228.41	0.741	8207.72	60.02	0.857	52.88	0.877	87.7

Table 4. The evaluated electrical parameters obtained by using EIS studies of 316LN stainless steel.

pH	**C_{inh}(μM)**	**R_s(Ω cm^{-2})**	**R_{po}(Ω cm^{-2})**	***CPE_{po}***		**R_{ct}(Ω cm^{-2})**	***CPE_{ct}***		**C_{dl}(μF cm^{-2})**	θ	***IE*(%)**
				$Q_{po} \times 10^{-6}$ (s^n Ω^{-1} cm^{-2})	**n_1**		**$Q_{ct} \times 10^{-6}$ (s^n Ω^{-1} cm^{-2})**	**n_2**			
8	Blank	6.71	73.11	2072.28	0.969	707.55	270.31	0.819	191.05	–	–
	5	4.29	70.14	1719.24	0.680	1171.30	240.35	0.727	151.10	0.395	39.5
	15	5.92	180.08	1237.15	0.959	1605.20	159.71	0.829	121.59	0.559	55.9
	25	7.21	301.04	860.41	0.561	2071.21	129.89	0.808	100.14	0.658	65.8
	50	6.28	504.01	509.71	0.840	2888.32	99.76	0.805	75.17	0.755	75.5
10	Blank	5.70	62.71	2990.3	0.668	848.54	220.02	0.798	139.78	–	-
	5	5.98	78.66	1629.71	0.491	1487.36	155.75	0.851	120.17	0.429	42.9
	15	4.39	189.85	1168.44	0.829	2091.41	130.24	0.772	90.15	0.594	59.4
	25	8.51	320.17	840.11	0.466	3105.66	100.42	0.753	66.42	0.726	72.6
	50	6.52	522.33	379.05	0.809	4855.33	80.15	0.771	60.78	0.825	82.5
12	Blank	7.92	69.96	990.21	0.919	1205.84	115.21	0.838	75.84	-	-
	5	6.42	99.81	720.14	0.605	2574.33	78.21	0.851	60.18	0.531	53.1
	15	7.30	239.77	579.42	0.948	3987.37	48.30	0.805	29.89	0.697	69.7
	25	7.79	479.18	379.15	0.702	7588.74	36.33	0.792	25.75	0.841	84.1
	50	7.89	700.11	120.25	0.839	18278.20	29.47	0.686	23.87	0.934	93.4

As it can be observed from Tables 3 and 4, with increasing inhibitor concentration, the double layer capacitance decreases and the charge transfer resistance increases which is associated with an improvement in the 'blanketing' property of the film. The surface coverage and inhibition efficiency are also increased with an increase in inhibitor concentration because it enhances the adsorption of inhibiter molecules at the surface of reinforcement steel which blocks the activation activity on the steel surface and increases the thickness of the protective film on the metal-solution interface [24, 52]. The charge transfer resistance is decreased with the decreasing the pH value. This is related to the dissolution or de-passivation of passive film that leads to localized attack of Cl^- on the metal surface [53]. A calcium nitrite concentration of 50 µM shows 87.7% and 93% inhibition efficiency at pH 12 at room temperature for API X120 carbon steel and 316LN stainless steel, respectively.

Moreover, the decrease in C_{dl} with the increasing the inhibitor concentration is caused by an increase in the thickness of the electric double layer that can act as a physical barrier between the steel surfaces and the corrosive environment [54], which can be described using the Helmholtz model as the following equation [40]:

$$\delta_{ads} = \frac{\varepsilon\varepsilon_0 A}{C_{dl}} = \frac{\varepsilon\varepsilon_0 A}{Q_0 \omega^{(n-1)}} \qquad (7)$$

Where δ_{ads} is the thickness of the adsorbed layer of inhibitor on the steel surface, A indicates the cross-sectional area of the electrode exposed to the corrosive medium, ε_o is the permittivity of air, and ε is the local dielectric constant. Thus, the Helmholtz model indicates that the thickness of protective layer is inversely proportional to C_{dl} and capacitance constant which indicates that the decrease of the C_{dl} can be attributed to the increase of the adsorbed layer of inhibitor with increasing the inhibitor concentration.

A comparison between the electrochemical corrosion behavior of API X120 carbon steel and 316LN stainless steel reinforced concrete reveals that when carbon steel and stainless steel are subjected to aggressive environments, the corrosion rate in carbon steel is higher than that in stainless steel. Results indicate a remarkable decrease in the lifetime of the structure concrete and damage due to reinforcement corrosion of API X120 carbon steel, implying an increase in the cost associated with monitoring and maintenance [55]. Studies suggested the indicating the higher amount of chromium into the 316LN stainless steel structure can help to create stable passive layers due to formation the CrO_3 and $Cr(OH)_{3\ in}$ passive film [56]. Therefore, replacing the API X120 carbon steel reinforcement with 316LN stainless steel can decrease the corrosion rate and can also considerably decrease the costs related to expensive equipment for rehabilitation.

Figure 6 shows the SEM images of API X120 carbon steel and 316LN stainless steel reinforced concrete that were immersed in the pH 12 of a 3.5%wt NaCl solution for 24 hours at room temperature without and with 50µM of calcium nitrite. As observed, the surface of reinforcement steel specimens in 3.5% wt NaCl solution without calcium nitrite shows high roughness and pitting corrosion due to highly aggressive media and Cl^- attack on the passive layer. SEM of reinforcement steel specimens in 3.5%wt NaCl solution containing 50 µM of calcium nitrite depicts smoother areas and less corroded surfaces, demonstrating the protective effect of calcium nitrite as a power corrosion inhibitor. Additionally, the comparison between the SEM images of API X120 carbon steel and 316LN stainless steel reveals that the API X120 carbon steel sample shows more damaged surface and multi-point

corrosion pits than the 316LN stainless steel, which increases the chance of extremely localized corrosion and enhances the corrosion rate.

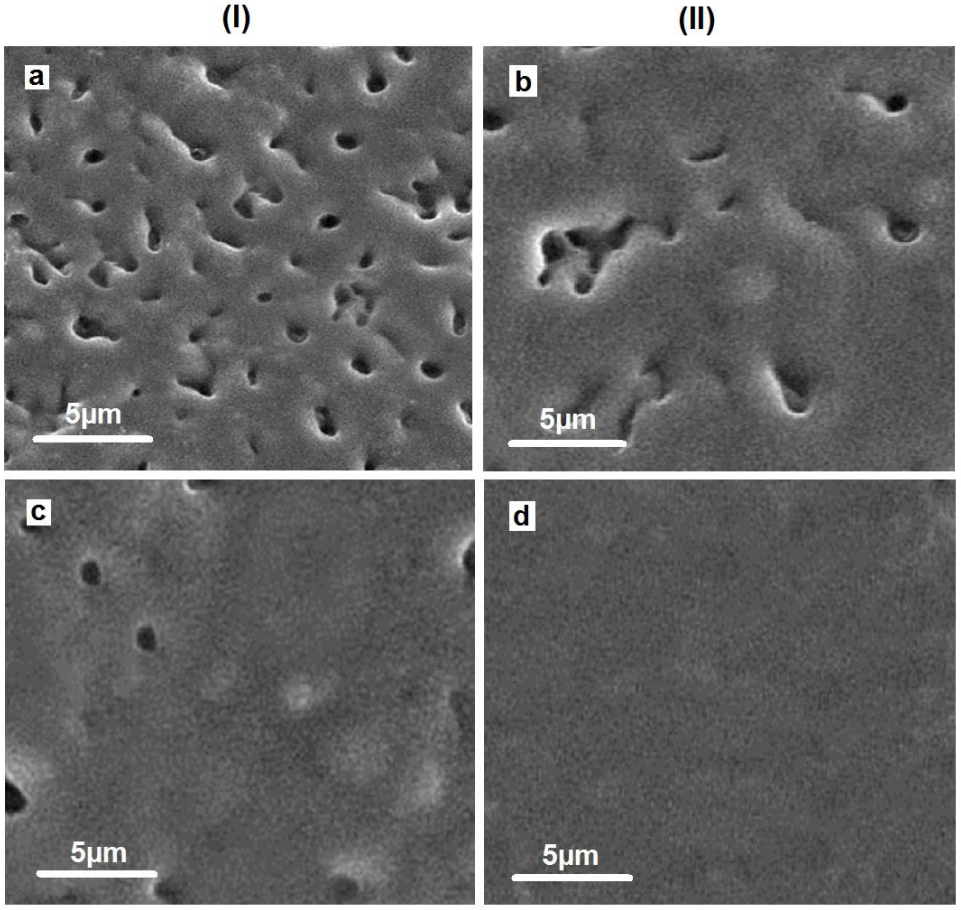

Figure 6. SEM images of API X120 carbon steel (column I) and 316LN stainless steel (column II) immersed in the pH 12 of 3.5% wt NaCl solution for 24 hours at room temperature (a and b) without and (c and d) with 50 µM of calcium nitrite.

4. CONCULUSION

This study was conducted to study the corrosion behavior of API X120 carbon steel and 316LN stainless steel reinforced concrete in the marine environment with calcium nitrite as an inhibitor. The results of EIS studies showed that the double-layer capacitance decreases and charge-transfer resistance increases increasing the inhibitor concentration which is associated with an improvement in the 'blanketing' property of the film. The inhibition efficiency and surface coverage are also increased with an increase in inhibitor concentration. A comparison between the corrosion behaviors of API X120 carbon steel and 316LN stainless steel reinforced concrete indicated to the higher inhibition efficiency of 316LN stainless steel in different inhibitor concentrations, and API X120 carbon steel showed a remarkable decrease in the lifetime of the structure concrete and damage. The results of the SEM study also indicated the more damaged surface of API X120 carbon steel and multi-point

corrosion pit than 316LN stainless steel, which increases the chance of extremely localized corrosion and enhances the corrosion rate. Therefore, replacing the API X120 carbon steel reinforcement with 316LN stainless steel can decrease the corrosion rate and can also considerably decrease the costs related to expensive equipment for rehabilitation.

References

1. T. Alexandru, B. Marinela, D. Laura and B. Irina, *Procedia Manufacturing*, 32 (2019) 253.
2. F. Chen, Z. Jin, E. Wang, L. Wang, Y. Jiang, P. Guo, X. Gao and X. He, *Scientific Reports*, 11 (2021) 1.
3. Y. Yu, Y. Zhao, Y.-L. Qiao, Y. Feng, W.-L. Li and W.-D. Fei, *Journal of Materials Science & Technology*, 84 (2021) 10.
4. H. Salehi and R. Burgueño, *Engineering structures*, 171 (2018) 170.
5. H. Huang, M. Huang, W. Zhang, S. Pospisil and T. Wu, *Journal of Structural Engineering*, 146 (2020) 04020157.
6. K. Li, D. Zhang, Q. Li and Z. Fan, *Cement and Concrete Research*, 115 (2019) 545.
7. J. Zhu, Y. Chen, L. Zhang, B. Guo, G. Fan, X. Guan and R. Zhao, *Journal of Cleaner Production*, 295 (2021) 126405.
8. F. Cui, H. Zhang, M. Ghosn and Y. Xu, *Engineering Structures*, 155 (2018) 61.
9. M.Z.Y. Ting, K.S. Wong, M.E. Rahman and S.J. Meheron, *Journal of Cleaner Production*, 278 (2021) 123383.
10. W. Green, *Corrosion Engineering, Science and Technology*, 55 (2020) 289.
11. A.B. Kale, B.-K. Kim, D.-I. Kim, E. Castle, M. Reece and S.-H. Choi, *Materials Characterization*, 163 (2020) 110204.
12. D.-C. Feng, S.-C. Xie, Y. Li and L. Jin, *Structural Safety*, 89 (2021) 102061.
13. W. Zhang, Z. Tang, Y. Yang, J. Wei and P. Stanislav, *Journal of Structural Engineering*, 147 (2021) 04021055.
14. Y. Yan, L. Feng, M. Shi, C. Cui and Y. Liu, *Food chemistry*, 306 (2020) 125589.
15. P. Gatheeshgar, K. Poologanathan, S. Gunalan, K.D. Tsavdaridis, B. Nagaratnam and E. Iacovidou, *Journal of Building Engineering*, 32 (2020) 101607.
16. F.-x. Chen, Y.-c. Zhong, X.-y. Gao, Z.-q. Jin, E.-d. Wang, F.-p. Zhu, X.-x. Shao and X.-y. He, *Scientific Reports*, 11 (2021) 1.
17. S. Ahmad, *Cement and concrete composites*, 25 (2003) 459.
18. H. Huang, M. Huang, W. Zhang and S. Yang, *Structure and Infrastructure Engineering*, 17 (2020) 1.
19. X. Tang, J. Wu, W. Wu, Z. Zhang, W. Zhang, Q. Zhang, W. Zhang, X. Chen and P. Li, *Analytical chemistry*, 92 (2020) 3563.
20. M.H. Moayed, Z. Abbaspour and M. Sadeghian, *International Journal of Engineering*, 22 (4) (2009) 369
21. I. Danaee, S. RameshKumar, M. RashvandAvei and M. Vijayan, *Materials Research*, 23 (2020) 1.
22. Y. Orooji, B. Tanhaei, A. Ayati, S.H. Tabrizi, M. Alizadeh, F.F. Bamoharram, F. Karimi, S. Salmanpour, J. Rouhi and S. Afshar, *Chemosphere*, 281 (2021) 130795.
23. H.S. Ryu, C.G. Lim, T.W. Kang, S. Lim, H.T. Kim and S.H. Shin, *Advances in Materials Science and Engineering*, 2019 (2019) 1.
24. E. Ituen, O. Akaranta and A. James, *Journal of King Saud University - Engineering Sciences*, 31 (2019) 191.

25. K. Kim, H. Kim, H. Chang, B. Lim, H. Park and Y. Kim, *Advances in Materials Science and Engineering*, 2015 (2015) 1.
26. Y. Song, J. Liu, H. Wang and H. Shu, *International Journal of Corrosion*, 2019 (2019) 1.
27. P. Garcés, P. Saura, A. Méndez, E. Zornoza and C. Andrade, *Corrosion science*, 50 (2008) 498.
28. L. Abosrra, M. Youseffi and A. Ashour, *International Journal of Concrete Structures and Materials*, 5 (2011) 65.
29. V. Elfmarkova, P. Spiesz and H. Brouwers, *Cement and concrete Research*, 78 (2015) 190.
30. M. Seifan and A. Berenjian, *Applied microbiology and biotechnology*, 103 (2019) 4693.
31. D. Silva, H. Roman and P. Gleize, *Cement and concrete research*, 32 (2002) 1383.
32. C.H.D. Nieto, N.A. Palacios, K. Verbeeck, A. Prévoteau, K. Rabaey and V. Flexer, *Water research*, 154 (2019) 117.
33. M. Shehata, N.A. Ghany and A. El Hosary, *Egyptian Journal of Chemistry*, 59 (2016) 1127.
34. W. Chalee, P. Ausapanit and C. Jaturapitakkul, *Materials & Design*, 31 (2010) 1242.
35. J. Kim, W.J. McCarter and B. Suryanto, *Construction and Building Materials*, 192 (2018) 569.
36. A. Costa and J. Appleton, *Materials and Structures*, 32 (1999) 354.
37. S.-J. Kwon, H.-S. Lee, S. Karthick, V. Saraswathy and H.-M. Yang, *Construction and Building Materials*, 154 (2017) 349.
38. L. Teng, C. He, X. Pan, C. Liu and X. Chen, *International Journal of Electrochemical Science* 16 (2021) 2.
39. R.H. Tammam, A. Mogoda and M.H. Gharbawy, *International Journal of Electrochemical Science* 15 (2020) 8408.
40. K. Shahzad, M.H. Sliem, R.A. Shakoor, A.B. Radwan, R. Kahraman, M.A. Umer, U. Manzoor and A.M. Abdullah, *Scientific Reports*, 10 (2020) 4314.
41. X.-P. Wang, M. Shao, C.-Q. Ye, S.-G. Dong, R.-G. Du and C.-J. Lin, *Journal of Electroanalytical Chemistry*, 895 (2021) 115454.
42. L. Sun, C. Li, C. Zhang, Z. Su and C. Chen, *International Journal of Structural Stability and Dynamics*, 18 (2018) 1840001.
43. Y. Zhou, B. Gencturk, K. Willam and A. Attar, *Journal of Materials in Civil Engineering*, 27 (2015) 04014245.
44. Y. Xu, L. He, L. Yang, X. Wang and Y. Huang, *Corrosion*, 74 (2018) 1063.
45. Z. Wu, S. Wu, J. Bao, W. Qian, S. Karabal, W. Sun and P.J. Withers, *International Journal of Fatigue*, 151 (2021) 106317.
46. E. Volpi, A. Olietti, M. Stefanoni and S.P. Trasatti, *Journal of Electroanalytical Chemistry*, 736 (2015) 38.
47. Z. Chu, G.L. Plett, M.S. Trimboli and M. Ouyang, *Journal of Energy Storage*, 25 (2019) 100828.
48. C. Monticelli, A. Balbo, J. Esvan, C. Chiavari, C. Martini, F. Zanotto, L. Marvelli and L. Robbiola, *Corrosion science*, 148 (2019) 144.
49. Y. Li, D.D. Macdonald, J. Yang, J. Qiu and S. Wang, *Corrosion Science*, 163 (2020) Point defect model for the corrosion of steels in supercritical water: Part I, film growth kinetics.
50. A.B. Radwan, M.H. Sliem, N.S. Yusuf, N.A. Alnuaimi and A.M. Abdullah, *Scientific reports*, 9 (2019) 18115.
51. F. Gómez-Zamudio, R. Antaño-López, A. Rodríguez-López, T. Perez and E. Larios-Durán, *International Journal of Electrochemical Science* 11 (2016) 475.
52. Y. Xie, X. Meng, D. Mao, Z. Qin, L. Wan and Y. Huang, *ACS Applied Materials & Interfaces*, 13 (2021) 32161.
53. Y. Hoshi, S. Watanabe, H. Tokieda, I. Shitanda and M. Itagaki, *Materials Transactions*, 62 (2021) 655.
54. J.-Y. Kim, I. Shin and J.-W. Byeon, *Materials*, 14 (2021) 5016.

55. M. Rabi, K.A. Cashell, R. Shamass and P. Desnerck, *Engineering Structures*, 221 (2020) 111027.
56. M. Liu, X. Cheng, X. Li, Z. Jin and H. Liu, *Construction and Building Materials*, 93 (2015) 884.